Journal of Cardiovascular Computed Tomography 20 (2026) 247–255

Contents lists available at ScienceDirect

Journal of Cardiovascular Computed Tomography

journal homepage: www.JournalofCardiovascularCT.com

Research Paper

Automatic CT-based quantification of myocardial extracellular volume fraction and high ECV burden and their prognostic value for death and heart failure in patients with aortic stenosis: a real-world data analysis

Alberto Colombo [a], Anna Palmisano [b,c], Chiara Gnasso [b,c], Davide Vignale [b,c], Elisa Bruno [b], Marta Liberotti [a,c], Marco Metra [b], Matteo Montorfano [b,d], Francesco Maisano [b,e], Carlo Tacchetti [a,b,c], Antonio Esposito [a,b,c,*]

[a] San Raffaele AI Center (S-RACE), Vita-Salute San Raffaele University, Via Olgettina, 58, 20132 Milan, Italy
[b] School of Medicine, Vita-Salute San Raffaele University, Via Olgettina, 58, 20132 Milan, Italy
[c] Advanced Imaging for Personalized Medicine Unit, Experimental Imaging Center, IRCCS San Raffaele Scientific Institute, Via Olgettina, 60, 20132 Milan, Italy
[d] Department of Interventional Cardiology, IRCCS San Raffaele Scientific Institute, Via Olgettina 60, 20132 Milan, Italy
[e] Department of Cardiac Surgery, Heart Valve Center, IRCCS San Raffaele Scientific Institute, Via Olgettina, 60, 20132 Milan, Italy

ARTICLE INFO

Keywords:
Aortic valve stenosis
Transcatheter aortic valve replacement
Tomography, X-Ray computed
Extracellular volume
Image processing, Computer-assisted
Prognosis

ABSTRACT

Background: Computed tomography (CT)–based myocardial extracellular volume (ECV) assessment during transcatheter aortic valve implantation (TAVI) planning is prognostically informative but limited by operator-dependent workflows. We developed a fully automated, standardized pipeline for volumetric ECV quantification and a derived metric reflecting the burden of myocardial extracellular matrix expansion (hECV-B) and evaluated their association with clinical outcomes after TAVI.

Methods: In a single-centre study of consecutive pre-TAVI cardiac CT examinations (10/2020–12/2023), a standardized pipeline performed automated cardiac segmentation, reorientation, co-registration and subtraction of late post-contrast and pre-contrast scans, and volumetric ECV mapping. hECV-B was defined as the fraction of left-ventricular voxels above prespecified ECV thresholds. Agreement between automated and manual (two radiologists) ECV was assessed with Bland–Altman analysis. Associations with a composite of all-cause death or heart-failure hospitalization at 12 months were evaluated using Kaplan–Meier/log-rank and multivariable Cox models adjusted for clinical and echocardiographic covariates.

Results: Of 664 screened patients, 438 were analysed (221 women and 217 men; median age 82 years). End-to-end processing was ≤4.5 min/patient. The composite outcome occurred in 74 patients (16.9%). Bland–Altman analysis showed negligible mean bias (<1%), with wider limits of agreement (−11.3%–13.1%). Elevated automated whole-LV ECV and hECV-B were independently associated with adverse outcomes, with risk predominantly concentrated at higher ECV values.

Conclusion: Fully automated CT-derived ECV and hECV-B assessment is feasible at scale and provides operator-independent markers of myocardial extracellular expansion associated with adverse outcomes after TAVI, supporting its potential role in standardized pre-procedural risk stratification in aortic stenosis.

Abbreviations: AIC, Akaike Information Criterion; AS, aortic stenosis; CT, computed tomography; CTA, computed tomography angiography; DICOM, Digital Imaging and Communications in Medicine; ECG, electrocardiogram; ECV, extracellular volume; hECV-B, high ECV burden; Hct, haematocrit; HU, Hounsfield unit; LAX, long axis; LV, left ventricle; LVEF, left ventricle ejection fraction; NIfTI, Neuroimaging Informatics Technology Initiative; PACS, Picture Archiving and Communication System; ROI, region of interest; SAX, short axis; TAVI, transcatheter aortic valve implantation; VOI, volume of interest.

* Corresponding author. Vita-Salute San Raffaele University, IRCCS San Raffaele Scientific Institute, Via Olgettina 58 – 60, 20132, Milan, Italy
E-mail addresses: colombo.alberto@unisr.it (A. Colombo), palmisano.anna@hsr.it (A. Palmisano), gnasso.chiara@hsr.it (C. Gnasso), vignale.davide@hsr.it (D. Vignale), bruno.elisa@hsr.it (E. Bruno), liberotti.marta@hsr.it (M. Liberotti), metra.marco@hsr.it (M. Metra), montorfano.matteo@hsr.it (M. Montorfano), maisano.francesco@hsr.it (F. Maisano), tacchetti.carlo@hsr.it (C. Tacchetti), esposito.antonio@hsr.it (A. Esposito).

https://doi.org/10.1016/j.jcct.2026.03.002
Received 9 January 2026; Received in revised form 23 February 2026; Accepted 12 March 2026
Available online 26 March 2026

1. Introduction

The clinical value of computed tomography (CT)-based extracellular volume (ECV) assessment in patients with aortic stenosis (AS) undergoing CT for transcatheter aortic valve implantation (TAVI) planning has been well established, demonstrating associations with all-cause mortality and hospitalization for heart failure, and has also proven useful for the detection of amyloidosis in this setting.[1,2]

Compared with cardiac magnetic resonance, the non-invasive reference standard for myocardial ECV assessment,[3,4] CT-derived ECV quantification offers important practical advantages: it can be derived from the same study used for standard TAVI planning by adding a delayed low-dose scan, without the need for additional contrast volume.[5–7]

Despite this strength, current CT-derived ECV assessment methods rely mainly on manual region-of-interest placement [7–9] or on semi-automated software solutions. [10–13] These workflows require expert operators, and exhibit user-level variability.[14,15] As a result, CT-derived ECV is still considered an emerging research technique, not yet recommended in the major European Society of Cardiology or American Heart Association guidelines for routine use. The main reasons why it remains confined to the category of promising but not yet clinically indicated biomarkers lie in the absence of standardized and fully automated methods for its extraction, which currently prevents the design of large prospective trials and, consequently, its potential clinical adoption. Broader adoption will likely require fully automated, operator-independent techniques capable of producing consistent volumetric myocardial characterization.

To date, no study has evaluated a fully automated, end-to-end pipeline for CT-derived ECV quantification in a large, real-world TAVI population. Furthermore, prior studies have focused primarily on single-slice or segmental average ECV values, whereas the increasing availability of high-resolution volumetric CT datasets allows for voxel-wise analysis and the possibility of novel biomarkers that capture the full spatial distribution of myocardial extracellular matrix expansion across the left ventricle.

Accordingly, the aims of this study were to develop a robust, fully automated end-to-end pipeline for volumetric ECV quantification; to derive a volumetric parameter reflecting the burden of myocardial extracellular matrix expansion (hECV-B) based on voxel-wise ECV threshold profiling; to evaluate the association of these automated biomarkers with 12-month all-cause mortality or heart-failure hospitalization in a large, real-world cohort of patients undergoing TAVI. By addressing current methodological limitations, this study aims to support the development of standardized, operator-independent CT-based myocardial tissue characterization.

2. Methods

2.1. Study population and study design

This single-centre observational study was approved by the institutional review board (CTMyoC 112/INT/2019) and registered at www.clinicaltrials.gov (NCT06029400). The study is a retrospective analysis of prospectively collected data and was conducted in accordance with the Declaration of Helsinki. Written informed consent was obtained from all participants.

Patients who underwent CT for TAVI planning at IRCCS San Raffaele Hospital between October 2020 and December 2023 and subsequently underwent TAVI were considered for inclusion. Patients with a bicuspid aortic valve, prior aortic valve prosthesis, periprocedural complications or death during index hospitalization, or missing data required for ECV calculation were excluded.

2.2. CT data acquisition and reconstruction

CT examinations were performed on a second-generation dual-source scanner (SOMATOM Definition Flash, Siemens Healthineers, Erlangen, Germany). The CT protocol included pre-contrast and late post-contrast cardiac scans, both performed using prospective electrocardiogram (ECG)-gating at a fixed 280 ms delay from the R-wave peak, acquired before and 5 min after CT angiography (CTA), respectively. CTA consisted of a retrospectively ECG-gated cardiac CT immediately followed by an ultra-high pitch thoracic–abdominal scan, for cardiac assessment, device sizing, and vascular access evaluation. CTA acquisition was triggered by the contrast bolus arrival in the left ventricle. Technical details of the pre-contrast and late post-contrast scan are provided in Supplementary Table 1.

2.3. Manual ECV quantification

Manual ECV analysis was performed by two radiologists, Reader 1 (DV) and Reader 2 (CG), with 7 and 3 years of experience in cardiovascular imaging. Both readers were blinded to each other's measurements. For extracellular volume (ECV) quantification, late post-contrast CT attenuation values (in Hounsfield units, HU) of the myocardium were obtained by placing a region of interest (ROI) larger than 2 cm^2 within the interventricular septum on a mid-ventricular slice, avoiding areas of beam hardening, streak artefacts, or myocardial scars. Blood pool attenuation was measured on the same slice by placing an ROI larger than 1 cm^2 within the left ventricular cavity. Pre- and late post-contrast CT scans were rigidly co-registered using the picture archiving and communication system (Enterprise Imaging, Agfa HealthCare, Belgium), after which the myocardial and blood pool ROIs were transferred to the pre-contrast images. ECV was then calculated using the following formula:

$$ECV = (1 - Hct)\frac{\Delta HU_{myo}}{\Delta HU_{blood}} \quad (1)$$

where Hct is the haematocrit value, and ΔHU_{myo} and ΔHU_{blood} represent the change in attenuation of myocardium and blood pool before and after contrast administration. Hct values were obtained from blood samples within 24 hours of the CT scan.

2.4. Automatic ECV and hECV-B quantification

A fully automatic pipeline was developed to quantify ECV using the subtraction method,[16] given Hct, and pre- and late post-contrast cardiac CT scans. The pipeline comprises four steps (Fig. 1). A detailed description of image post-processing methods and hardware specifications are available in the Supplementary Material.

DICOM images were exported from PACS, converted into NIfTI format, and cardiac structures of interest were segmented directly on late post-contrast CT using the pre-trained nnU-Net *TotalSegmentator* model ("heartchambers_highres" task).[17] Segmented structures included the left ventricular (LV) myocardium, cardiac chambers, and aorta. The interventricular septum and mitral valve plane were derived through logical operations. All segmentations and images were then resampled to an isotropic voxel size of 1 mm^3.

Segmentations were post-processed to define myocardial orientation and volumes of interest (VOIs). Short-axis views were generated by estimating the LV long axis via principal component analysis and applying an affine rotation. The LV myocardium was refined using 1 mm erosion to exclude boundary voxels and regions adjacent to valves; robustness of ECV measurements to boundary modifications was also assessed using 2 mm erosion. The myocardium was divided according to the 16-segment AHA model.

Two myocardial VOIs were analysed: whole-LV (segments 1–16) and septal baso-medial regions (segments 2, 3, 8, 9). Two spherical VOIs (1.5 cm diameter) were positioned in the blood pool: one at the centre of mass of the left atrium and the other at the centre of mass of the basal LV blood pool to estimate ΔHU_{blood}.

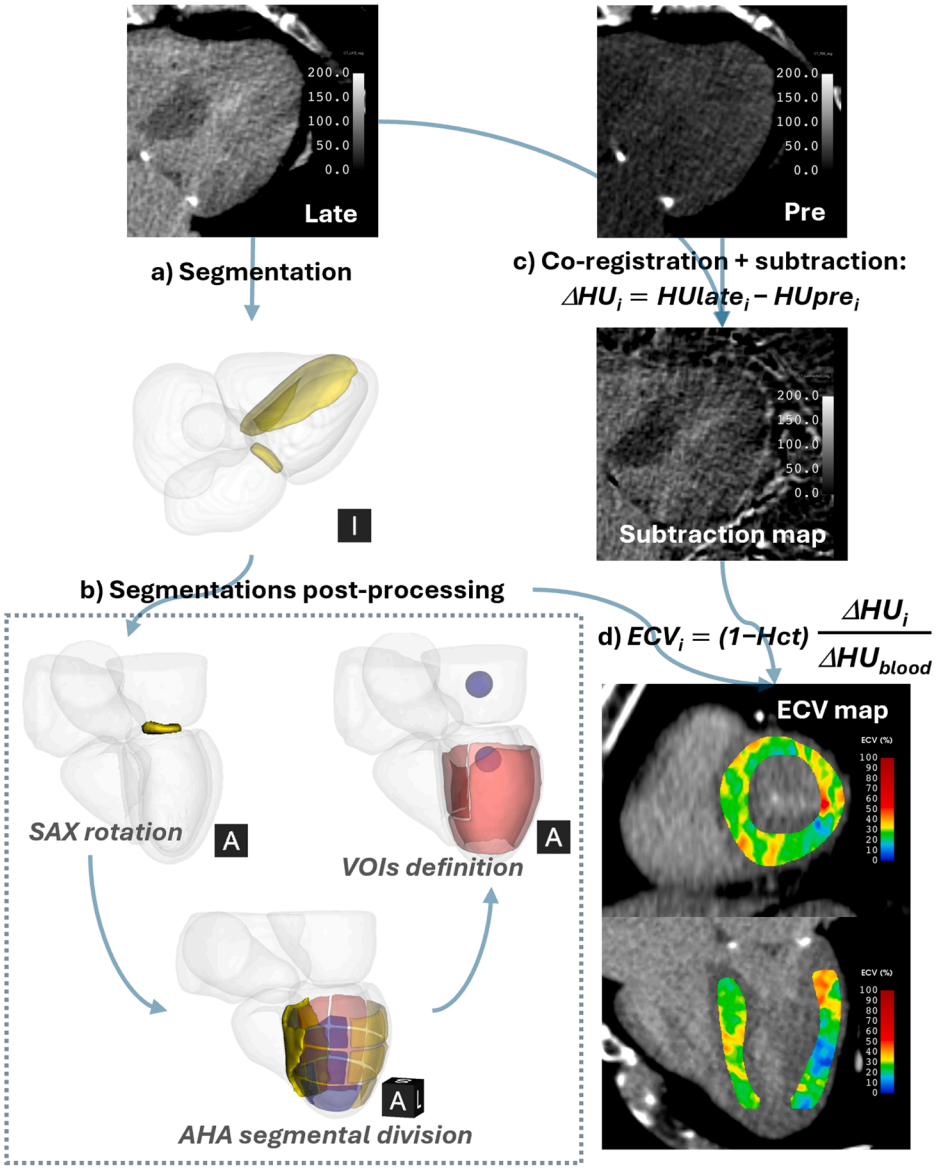

Fig. 1. Automated ECV quantification pipeline. a) Segmentation of cardiac structures on the late post-contrast CT using a pre-trained nnU-Net, with generation of support segmentations (interventricular septum and mitral valve plane, shown in yellow) via morphological and logical operations; b) Post-processing of segmentations, including estimation of the long-axis orientation to generate short-axis (SAX) views, myocardial division according to the 16-segment AHA model (apex excluded), and definition of myocardial and blood-pool volumes of interest (VOIs); c) Rigid and deformable co-registration of the pre-contrast (Pre) CT to the late post-contrast (Late) CT and creation of the voxel-wise subtraction map; d) Computation of the extracellular volume (ECV) map.

Pre-contrast images were co-registered to late post-contrast images using rigid and deformable transformations. Then, a subtraction map was created by calculating

$$\Delta HU_i = HUlate_i - HUpre_i \quad (2)$$

for each voxel i, where $HUlate_i$ and $HUpre_i$ are the attenuations in HU measured on late post-contrast and pre-contrast images, respectively, and ΔHU_i is the corresponding change in attenuation.

Finally, the voxel-wise ECV map was obtained by scaling each voxel i of the subtraction map using the formula

$$ECV_i = (1 - Hct)\frac{\Delta HU_i}{\Delta HU_{blood}} \quad (3)$$

where Hct is the haematocrit value, ΔHU_i is the differential attenuation in HU for each voxel i, ΔHU_{blood} is a scalar representing the differential attenuation in HU within the blood pool before and after contrast administration, calculated as the median differential attenuation within the two spherical VOIs placed in the basal LV and left atrium cavities, ECV_i is the ECV value for voxel i. Mean ECV values were extracted for whole-LV and septal VOIs.

ECV profiling was performed by calculating the proportion of LV myocardial voxels exceeding thresholds from 20% to 70%, encompassing the physiological and pathological spectrum of myocardial ECV values, from healthy myocardium to pathological expansion up to the levels observed in advanced amyloidosis.[2] hECV-B was computed as the proportion of LV voxels exceeding a given ECV threshold (identified using the approach described in the Statistical analysis section), integrating both the extent and severity of extracellular matrix expansion.

2.5. Outcome

The outcome was a composite of all-cause mortality (death) and heart failure hospitalization (HF), evaluated at 12 months after TAVI. Events occurring after the observation period were censored.

2.6. Statistical analysis

Descriptive statistics of the study population were calculated, and the association of continuous and categorical variables with event occurrence was evaluated using t-tests or Mann-Whitney U tests as appropriate (based on the Shapiro–Wilk test result) and Chi-square tests, respectively.

To compare manual and automatic ECV measures, correlation was evaluated using the Pearson correlation coefficient and linear regression, whereas agreement was assessed by calculating bias and 95% limits of agreement using the Bland–Altman method. Agreement between ECV measures obtained using 1 mm and 2 mm erosion was also assessed.

Group differences in ECV profiling were evaluated using the energy distance, a non-parametric measure of dissimilarity based on average pairwise Euclidean distances between patient-specific curves, as described by Székely et al.[18] The energy statistic was estimated using the unbiased V-statistic estimator, and statistical significance of dissimilarity between curves was assessed using a permutation test with 2000 random label reassignments.

Survival was first estimated using the Kaplan–Meier method. To identify cutoff values for continuous variables, a log-rank test was applied within a 4-fold stratified cross-validation framework, repeated 20 times for robustness. In each fold, 30 candidate cutoffs were randomly sampled from the variable's dynamic range. The cutoff that yielded the widest separation between survival curves (i.e., the lowest average p-value on the validation sets) while keeping at least 20% of patients in the minority group was selected. The optimal hECV-B cutoff was then derived at the identified ECV threshold using the same method.

Independent associations of ECV and hECV-B with the composite outcome were assessed using Cox proportional hazards models. Univariable analyses were performed for each predictor of interest. Multivariable models were subsequently fitted, each incorporating age, sex, EuroSCORE II, left ventricular ejection fraction, and aortic valve mean gradient as covariates, along with one ECV-related variable at a time. Additional multivariable models were fitted to evaluate the incremental prognostic value of whole-LV ECV over septal ECV measured either manually or automatically, with the same covariates retained. Model fit was compared using the likelihood ratio test and the Akaike Information Criterion (AIC). ΔAIC was defined as the AIC of the base model minus that of the full model; negative values indicate improved fit with the addition of the variable of interest. Multicollinearity among candidate predictors was evaluated using the variance inflation factor (cutoff = 5). To assess whether the prognostic effect of ECV was consistent across patient subgroups, interaction terms between ECV and EuroSCORE II, left ventricular ejection fraction, and mean aortic gradient were tested separately in multivariable models.

Finally, sensitivity analyses were conducted by progressively restricting the cohort to patients with whole-LV ECV ≤45%, ≤40%, and ≤35%, with multivariable Cox models refitted using the same covariate adjustment.

All statistical analyses were performed using Python (version 3.9.13). A two-sided significance level of $p = 0.05$ was used for all hypothesis tests.

3. Results

3.1. Population characteristics

Six hundred sixty-four patients underwent CT for TAVI planning at our institution in the observation period and subsequently underwent TAVI. As illustrated in the study flowchart (Fig. 2), 15 patients were excluded for having a bicuspid aortic valve, 18 for prior valvular surgery, 4 had intraprocedural complications, and 5 died during the TAVI procedure or index hospitalization. One patient with severe aortic insufficiency and one with amyloidosis associated with aortic stenosis were also excluded. Data required for ECV calculation were not available in 34 patients (the cardiac pre-contrast scan, the late post-contrast scan and the haematocrit value were missing in 4, 29, and 1 patient, respectively), while CT acquisitions were of insufficient quality for ECV quantification in 14 patients. Finally, 135 patients were lost at follow-up, resulting in 438 patients included in the analysis. To assess potential selection bias, baseline clinical characteristics were compared between included patients and the 116 of 135 patients lost to follow-up for whom clinical data were available (Supplementary Table 2).

The median follow-up was 15.6 months (IQR: 13.5–18.3), during which 93 of 438 patients (21.2%) experienced the composite outcome. Within the considered 12-month period, 57 deaths (10.7%) occurred, and the composite outcome of death or hospitalization for heart failure was observed in 74 patients (16.9%).

Population characteristics at the time of the CT examination for the complete cohort and with respect to the occurrence of the composite outcome are reported in Table 1. The median (IQR) age was 82.0 (78.0,85.0), half of the patients (50.5%) were females, and the median EuroSCORE II was 4.7 (2.9, 7.9). The parameters derived from CT for the complete cohort and stratified by outcome are summarized in Table 2.

3.2. Processing time and ECV findings

The automatic pipeline was successfully applied to the complete population. Processing times per-patient were as follows: segmentation of cardiac structures, ≤120 s; reorientation and VOI definition, ≤20 s; resampling and co-registration, ≤120 s; subtraction map generation and ECV and hECV-B computation, ≤10 s. Total end-to-end automatic processing time was ≤4.5 min.

ECV was consistently higher in patients who experienced the composite outcome compared to those who did not, and the difference was statistically significant for most measures, including septal and whole-LV ECV by automatic analysis (29.4% vs 31.6%, $p = 0.033$ and 29.3% vs 32.5%, $p = 0.001$, respectively) and septal measures by reader R2 (28.0 vs 30.4, $p = 0.002$), but not for septal ECV measures by reader R1 ($p = 0.148$). Example cases are provided in Fig. 3.

3.3. ECV measurement agreement

Agreement of ECV measurements was assessed in patients with readings from both readers ($n = 311$; Fig. 4). R1 had measurements for all patients. Measures of ECV from readers R1 and R2 were unbiased, and agreement was moderate, with Bland–Altman limits of agreement of ±9.3% and a Pearson correlation coefficient of 0.60 ($p < 0.001$). Similar

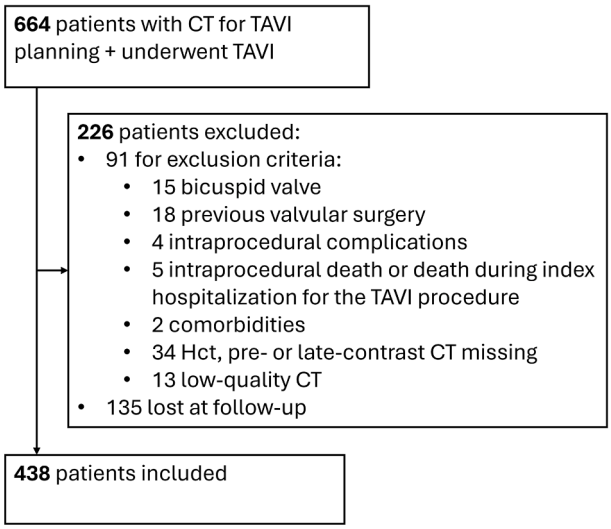

Fig. 2. Patient selection flowchart.

Table 1
Patients' characteristics at the time of the pre-TAVI CT examination.

		Overall	Death or HF −	Death or HF +	P-Value
n		438	364	74	
Age (years)		82.0 [78.0,85.0]	82.0 [78.0,85.0]	82.5 [78.0,86.0]	0.224
Sex	**Female**	221 (50.5)	196 (53.8)	25 (33.8)	0.003
	Male	217 (49.5)	168 (46.2)	49 (66.2)	
BMI (kg/m^2)		25.0 [23.0,28.0]	25.0 [23.0,28.0]	24.0 [22.0,26.8]	0.082
Diabetes	**No**	309 (70.5)	268 (73.6)	41 (55.4)	0.003
	Yes	129 (29.5)	96 (26.4)	33 (44.6)	
Hypertension	**No**	86 (19.6)	71 (19.5)	15 (20.3)	1.000
	Yes	352 (80.4)	293 (80.5)	59 (79.7)	
Hypercholesterolaemia	**No**	190 (43.4)	155 (42.6)	35 (47.3)	0.537
	yes	248 (56.6)	209 (57.4)	39 (52.7)	
Current smoker	**No**	416 (95.0)	346 (95.1)	70 (94.6)	0.775
	Yes	22 (5.0)	18 (4.9)	4 (5.4)	
Former smoker	**No**	313 (71.5)	262 (72.0)	51 (68.9)	0.697
	Yes	125 (28.5)	102 (28.0)	23 (31.1)	
CKD	**No**	357 (81.5)	308 (84.6)	49 (66.2)	<0.001
	Yes	81 (18.5)	56 (15.4)	25 (33.8)	
Previous revascularization	**CABG**	17 (3.9)	12 (3.3)	5 (6.8)	0.559
	CABG + PCI	11 (2.5)	9 (2.5)	2 (2.7)	
	No	323 (73.7)	271 (74.5)	52 (70.3)	
	PCI	87 (19.9)	72 (19.8)	15 (20.3)	
LF-LG aortic stenosis	**No**	370 (84.5)	317 (87.1)	53 (71.6)	0.002
	Yes	68 (15.5)	47 (12.9)	21 (28.4)	
BNP (ng/dL)		1115.0 [476.2,2606.8]	995.0 [435.0,2434.0]	1800.0 [685.5,3174.0]	0.028
TnT (ng/L)		24.0 [16.5,39.2]	23.0 [16.1,34.6]	38.5 [20.1,52.7]	0.001
EuroSCORE II (%)		4.7 [2.9,7.9]	4.7 [2.8,7.6]	5.0 [4.3,11.7]	0.012

Table 2
Imaging characteristics derived from pre-TAVI CT examination.

n	Overall	Death or HF −	Death or HF +	P-Value
	438	364	74	
Echocardiography variables				
LVEF (%)	59.0 [54.0,64.0]	60.0 [55.0,64.0]	55.0 [45.5,61.0]	<0.001
AVA indexed (cm^2/m^2)	0.39 [0.33,0.47]	0.39 [0.33,0.47]	0.42 [0.34,0.50]	0.078
AV mean gradient (mmHg)	44.0 [39.0,53.0]	44.0 [40.0,54.0]	41.0 [28.2,47.0]	<0.001
IVS thickness (mm)	13.0 [12.0,14.0]	13.0 [12.0,14.0]	13.0 [12.0,14.0]	0.471
Relative wall thickness	0.50 [0.44,0.58]	0.50 [0.44,0.58]	0.48 [0.43,0.55]	0.085
CT variables				
LV-EDV indexed (mL/m^2)	84.1 [70.8,96.5]	82.6 [70.6,95.8]	88.3 [71.8110.8]	0.033
LVEF (%)	62.0 [50.2,69.0]	63.0 [52.0,70.0]	55.0 [39.0,63.0]	<0.001
LV mass indexed (g/m^2)	90.0 [75.7109.2]	89.6 [75.5107.4]	96.8 [77.5116.7]	0.037
RV-EDV indexed (mL/m^2)	86.8 [74.8,97.3]	85.7 [73.8,94.9]	94.8 [83.2114.2]	<0.001
RV-EF (%)	49.0 [42.0,56.0]	50.0 [44.0,56.0]	44.0 [37.0,52.0]	<0.001
AV calcium score (AU)	2160 [1495,3271]	2171 [1460,3335]	2124 [1601,3077]	0.918
CACS (AU)	603 [226,1574]	552 [200,1445]	1155 [440,2232]	<0.001
$ECV_{S.R1}$ (%)	28.0 [26.0,32.0]	28.0 [25.8,32.0]	29.0 [26.2,33.8]	0.148
$ECV_{S.R2}$ (%)	28.7 [25.6,31.9]	28.0 [25.4,31.4]	30.4 [27.0,34.1]	0.001
$ECV_{S.manu}$ (%)	28.5 [25.5,32.1]	28.0 [25.3,32.0]	30.1 [26.5,33.9]	0.019
$ECV_{S.auto}$ (%)	29.6 [25.4,34.5]	29.4 [25.3,33.9]	31.6 [25.5,37.8]	0.033
$ECV_{LV.auto}$ (%)	29.7 [26.1,33.8]	29.3 [25.9,33.1]	32.5 [27.3,38.0]	0.001

agreement was observed when comparing the average of manual measures with the automatic measures, with Bland–Altman bias below 1% and limits of agreement within −11.3–13.1%, and Pearson correlation coefficients of 0.55 and 0.45 (both $p < 0.001$) for septal and whole-LV ECV, respectively.

ECV measurements from 1-mm and 2-mm eroded boundaries showed excellent agreement for both septal and whole-LV regions, with bias below 0.03% and limits of agreement within −0.4–0.5% (Supplementary Fig. 1).

3.4. ECV profile and hECV-B analysis

The fraction of left-ventricular myocardial voxels exceeding each ECV cutoff between 20% and 70% was consistently higher in patients who experienced the composite outcome compared to those who did not (Fig. 5). The separation between groups was most pronounced at ECV values between 28% and 40%, with an 8.2% peak in the absolute difference between voxel fractions at ECV = 33%. Consistent with the visual analysis, the non-parametric energy-distance test confirmed a statistically significant difference between the curves of the two groups (energy distance = 8.95, $p < 0.001$).

3.5. Survival analysis

In Kaplan-Meier survival analysis (Fig. 6), patients with a mean ECV higher than the identified cutoffs of 30% ($p = 0.006$) and 33% ($p \leq 0.006$) for manual and automatic measures, respectively, had a significantly increased risk of the composite endpoint. For the identified ECV cutoff, an hECV-B cutoff of 42.6% provided the best separation between survival curves ($p < 0.001$).

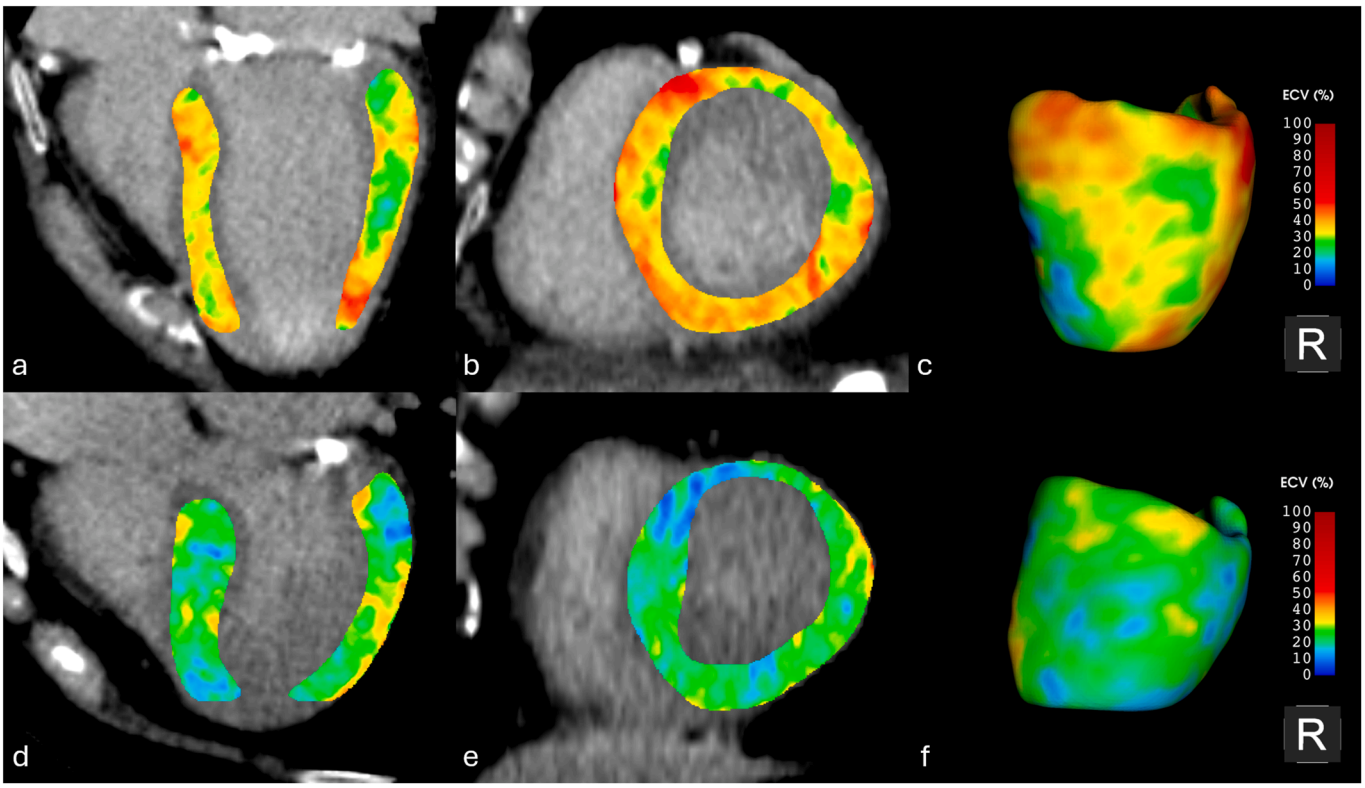

Fig. 3. Representative automated CT-derived extracellular volume (ECV) maps in two women with severe aortic stenosis. Panels a–c show a 66-year-old patient with elevated mean ECV (34.9%) who experienced the composite outcome. Long-axis, short-axis, and 3-dimensional reconstruction of the ECV map demonstrate diffusely increased myocardial ECV, consistent with more advanced extracellular matrix expansion. Panels d–f show a patient with lower mean ECV (24.2%) who remained event-free, with comparatively lower myocardial ECV values, consistent with limited extracellular expansion. Colour scale represents voxel-wise ECV percentage.

All variables were significantly associated with the outcome in univariable analysis. In multivariable analyses (Table 3), automatic ECV measures obtained from the whole-LV (1.04 [1.00–1.07], p = 0.028) and hECV-B (1.02 [1.00–1.03], p = 0.043) remained significantly associated with the composite outcome, whereas septal ECV measures, wether obtained manually (p = 0.469) or automatically (p = 0.375), were not.

No significant interaction was detected between whole-LV ECV and EuroSCORE II, LVEF, or mean aortic gradient (all p ≥ 0.38), suggesting that the prognostic effect of whole-LV ECV was consistent across the range of these variables. Whole-LV ECV provided independent and incremental prognostic value over septal ECV regardless of the septal measurement approach, whether manual (HR 1.04 [1.00–1.08], p = 0.041; ΔAIC −2.07) or automatic (HR 1.07 [1.01–1.13], p = 0.018; ΔAIC −3.44), and after adjustment for covariates (Supplementary Table 3). All variance inflation factors were low (maximum 2.61), suggesting no relevant collinearity among variables, even in models including whole-LV and septal ECV measures.

In sensitivity multivariable analyses progressively excluding patients with whole-LV ECV values ≤ 45%, ≤ 40%, and ≤ 35%, whole-LV ECV and hECV-B were no longer associated with the outcome (Supplementary Table 4). As progressively lower ECV cutoffs were applied, hazard ratios moved closer to 1.0, suggesting that the increased risk was largely concentrated among patients with the highest ECV values.

4. Discussion

This study demonstrates the feasibility and prognostic value of fully automated myocardial ECV quantification using routine pre- and late post-contrast cardiac CT in a large, real-world cohort of patients undergoing transcatheter aortic valve implantation (TAVI).

Our automated pipeline successfully processed imaging data from 438 TAVI patients, showing its practicality and broad clinical applicability. The end-to-end processing time—below 5 min for segmentation, reorientation, registration, subtraction, and ECV mapping—suggests that integration into routine workflows is achievable without substantial time burden. Because segmentation and co-registration are independent tasks, they could be parallelized to further shorten execution time. The algorithm is also adaptable to dual-energy or photon-counting CT acquisitions, where ECV quantification can be derived directly from iodine maps, eliminating the need for subtraction and co-registration, removing potential registration errors, and further reducing computational load.[6,16]

In Bland–Altman analysis, mean bias between automatic and manual measurements was negligible (<1%), and agreement was only marginally lower than manual inter-reader agreement. However, limits of agreement (±9–13%) were wider than previously reported. Smaller prior cohorts (≈20 patients) may have underestimated real-world variability, whereas our larger dataset (n = 438) better reflects routine practice.[9,19,20] In addition, our lower-dose protocol (160 vs 240–340 mAs at 120 kV) may have increased image noise and measurement dispersion. Methodological differences likely also contributed: manual septal measurements relied on small 2D regions of interest, favouring intrinsic homogeneity, whereas automated analysis used larger 3D volumetric regions of the medio-basal septum and whole-LV. Clinically, these limits exceed typical biological variability in AS (2–4%), limiting measurement method interchangeability for longitudinal follow-up or subtle phenotypic differentiation, but remain sufficient to distinguish AS from transthyretin amyloidosis cohorts, where differences are substantially larger (up to 20–30%).[2,19] Importantly, full automation eliminates inter-observer variability and enables consistent, scalable quantitative assessment.

Both the manual and automated ECV cutoffs identified in this study (30% and 33%, respectively) fall within the 95% confidence interval (28.5–33.7%) reported in a recent meta-analysis, in which the pooled

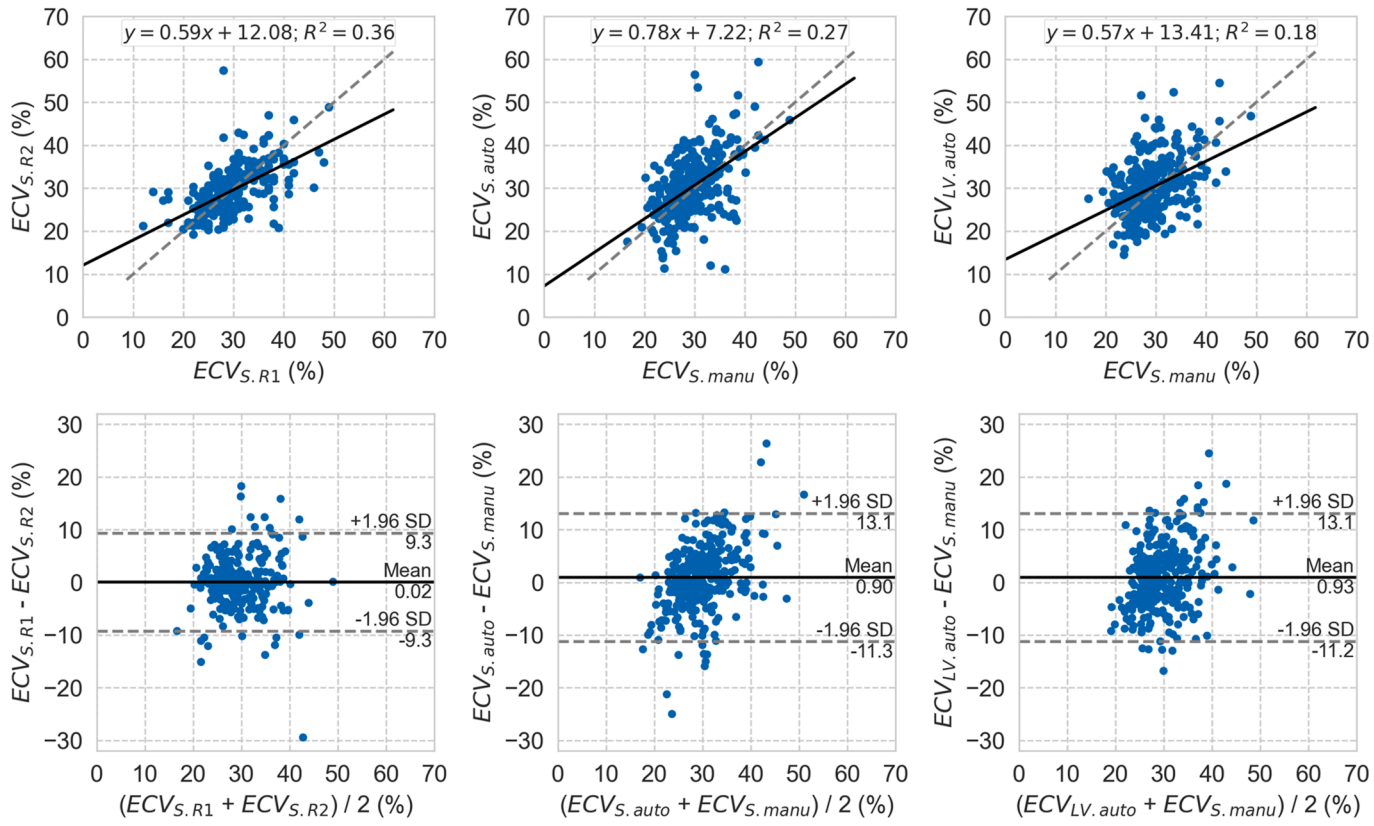

Fig. 4. Correlation and agreement between manual and automated ECV measurements. Top row: scatter plots with linear regression lines for septal ECV measured manually by (left) Readers 1 and 2, (centre) automated vs manual septal ECV, and (right) automated whole-LV vs manual septal ECV. The dashed line represents the line of identity. Bottom row: corresponding Bland–Altman plots showing mean bias and 95% limits of agreement for (left) inter-reader septal ECV, (centre) automated vs manual septal ECV, and (right) automated whole-LV vs manual septal ECV.

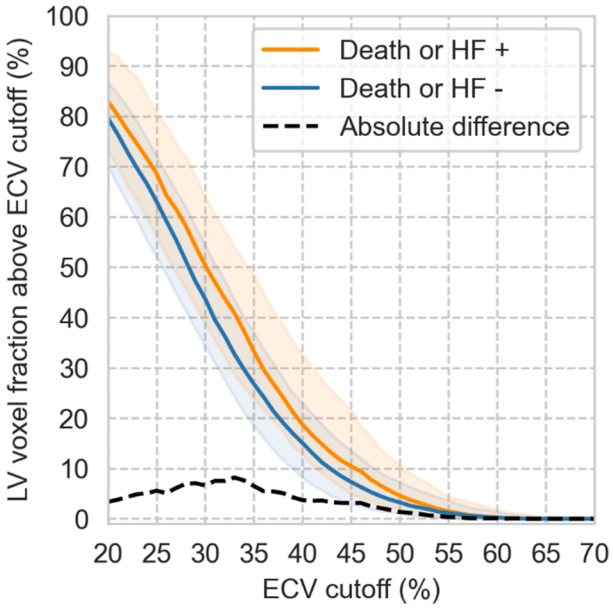

Fig. 5. Voxel-wise ECV-threshold profiles in patients with and without the composite outcome. Curves show the proportion of left-ventricular (LV) myocardial voxels exceeding each extracellular volume (ECV) cutoff from 20% to 70% for patients who experienced the composite outcome (orange) and those who did not (blue). Shaded bands represent interquartile ranges. The black dashed line shows the absolute difference between median curves at each threshold, indicating the range of maximal separation between groups.

CT-derived ECV threshold for defining elevated values and predicting prognosis was 30.7%.[1]

In our cohort, whole-LV ECV was independently associated with the outcome, while septal ECV was not. The superior prognostic performance of whole-LV metrics compared to septal ECV aligns with the notion that extracellular volume expansion in aortic stenosis is regionally heterogeneous, with documented base–apex and transmural gradients,[13] and that a global measure may better capture the extent of diffuse left ventricular remodelling than a regional surrogate limited to the septum. Septal ECV was significantly associated with outcomes in univariable analysis but, unlike prior reports, did not emerge as an independent predictor in multivariable models. Rather than a true inconsistency, this discrepancy may reflect methodological heterogeneity across studies that have evaluated the prognostic value of septal CT-derived ECV, a finding consistent with the substantial variability in covariate adjustment, cohort characteristics and follow-up duration.[7,11,13]

The absence of dedicated testing for transthyretin amyloidosis, with a previously reported prevalence of ~12% in patients with severe AS, likely led to inclusion of patients with concomitant dual pathology.[20] Although the independent association of ECV with outcomes has been confirmed in 'pure' AS cohorts with negative bone scintigraphy screening,[13,21] this limitation is shared by many studies evaluating the prognostic value of ECV in AS.[1,7,8,11] Notably, the loss of association between whole-LV ECV and hECV-B and the outcome in sensitivity analyses excluding patients with high whole-LV ECV values (>45%, >40%, and >35%) underscores the disproportionate event burden within the upper tail of the ECV distribution. These findings suggest that the prognostic signal is amplified at higher ECV values and is attenuated when extreme extracellular expansion is excluded.

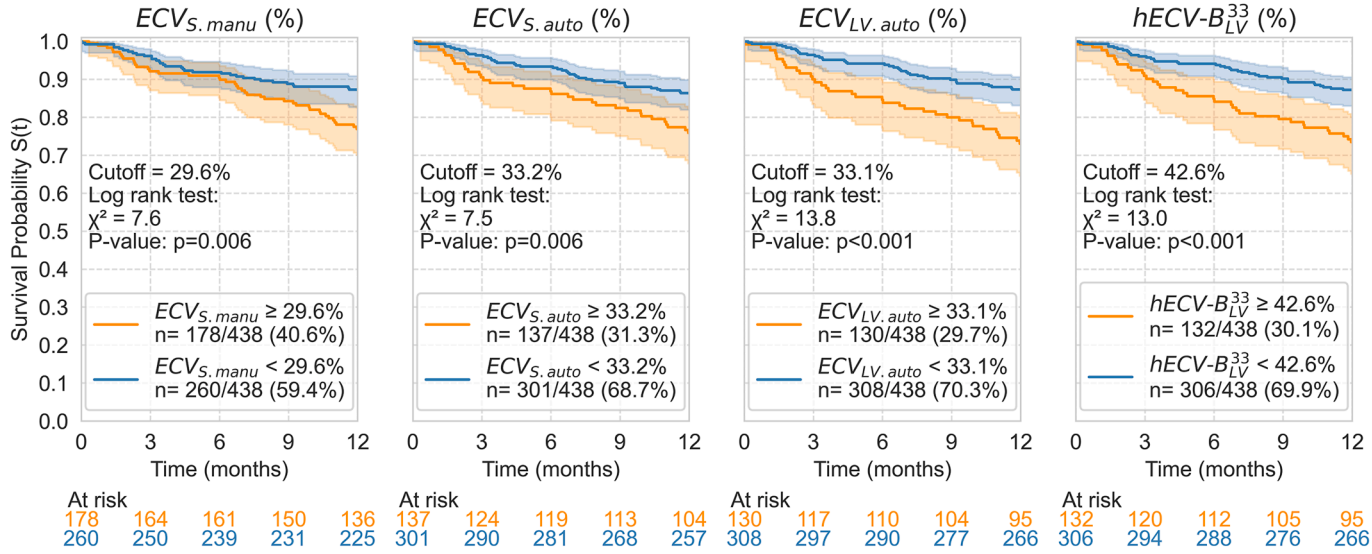

Fig. 6. Kaplan–Meier survival curves for the composite outcome according to manual and automated ECV measures and hECV-B. Panels show survival probability stratified by optimal cross-validated thresholds for (from left to right) manual septal ECV, automated septal ECV, automated whole-LV ECV, and LV hECV-B defined at the 33% ECV threshold. For each metric, the orange curve represents patients with values equal or above the identified cutoff, and the blue curve represents those below. Corresponding log-rank test statistics, p-values, and numbers at risk over time are shown below each panel.

Table 3
Univariable and multivariable Cox proportional hazard models.

	Univariable analysis HR (95%CI), P-value	Multivariable analysis[a] HR (95%CI), P-value	ΔAIC	LRT
$ECV_{S.manu}$ (%) (per 1% increase)	1.05 (1.01–1.09), p = 0.011	1.02 (0.97–1.06), p = 0.469	+1.488	χ^2 = 0.512, p = 0.474
$ECV_{S.auto}$ (%) (per 1% increase)	1.04 (1.01–1.07), p = 0.006	1.01 (0.98–1.04), p = 0.375	+1.226	χ^2 = 0.774, p = 0.379
$ECV_{LV.auto}$ (%) (per 1% increase)	1.07 (1.04–1.10), p < 0.001	1.04 (1.00–1.07), p = 0.028	−2.526	χ^2 = 4.526, p = 0.033
$hECV\text{-}B_{LV.33}$ (%) (per 1% increase)	1.03 (1.02–1.04), p < 0.001	1.02 (1.00–1.03), p = 0.043	−2.029	χ^2 = 4.029, p = 0.045

[a] Adjusted for age, sex, EuroSCORE II, LVEF measured at echocardiography and AV mean gradient.

From a pathophysiological perspective, diffuse interstitial remodelling and focal replacement fibrosis represent complementary stages of myocardial adaptation in aortic stenosis. Early pressure-overload remodelling is dominated by reactive interstitial expansion, whereas advanced disease is characterized by irreversible replacement fibrosis following myocyte loss.[22,23] In this context, voxel-wise ECV analysis provides a volumetric assessment of extracellular matrix expansion across the entire myocardium. By quantifying the proportion of left ventricular voxels exceeding a predefined ECV threshold, hECV-B reflects the extent and spatial distribution of myocardial extracellular matrix expansion. As such, it may encompass heterogeneous myocardial phenotypes characterized by increased extracellular volume, including advanced interstitial remodelling, foci of replacement fibrosis – which cardiac MRI studies have shown typically involve a limited proportion of the myocardium (2–8%),[24,25] and infiltrative processes. For example, prior CT data have found ECV values of 34 ± 4% in patients with early-stage transthyretin amyloidosis (Perugini score 1).[26] In our cohort, a hECV-B exceeding 43% of left ventricular voxels above the data-driven ECV threshold of 33% was independently associated with adverse outcomes after adjusting for clinical and echocardiographic parameters. This finding underscores the potential of volumetric ECV-derived metrics as complementary biomarkers that integrate both the magnitude and distribution of extracellular matrix expansion. As CT-derived ECV continues to evolve, such volumetric approaches may enable more comprehensive phenotyping of myocardial disease, with potential applications extending beyond TAVI to hypertensive heart disease, cardiomyopathy evaluation, and therapy monitoring. [2,27–29].

Cardiac MRI remains the reference standard for non-invasive myocardial tissue characterization. However, CT-derived ECV enables myocardial assessment within the routine TAVI planning examination, without additional contrast administration. Compared to MRI, CT is more widely available, requires shorter acquisition times, and is better tolerated in patients with claustrophobia or metallic implants.[25]

This study has several limitations. It was conducted at a single high-volume centre using a single scanner platform, which may limit generalizability. External validation across vendors, reconstruction kernels, and acquisition protocols is needed. We did not include histological or MRI-based ECV validation, preventing direct comparison of absolute ECV measures with gold-standard tissue characterization. Additionally, 20% of initially eligible patients were lost at follow-up. Although most baseline characteristics, including ECV, were comparable between included and excluded patients, small but statistically significant differences were observed in selected clinical and functional parameters (e.g., AV mean gradient, EuroSCORE II). These variables were adjusted for in multivariable analyses, but residual selection bias cannot be entirely excluded.

5. Conclusion

In conclusion, leveraging a robust, fully automated image-processing pipeline, we derived volumetric CT-based ECV maps and quantified myocardial extracellular matrix expansion in patients with aortic stenosis undergoing TAVI. Automated whole left ventricular ECV and hECV-B were feasible at scale and independently associated with 12-

month adverse outcomes, with risk predominantly concentrated among patients with higher ECV values. These findings support the potential of standardized, operator-independent CT-based myocardial tissue characterization to enhance pre-procedural risk stratification in TAVI candidates. Further multicentre validation is warranted to define its role across diverse myocardial phenotypes and clinical settings.

Data availability statement

Data are available from the corresponding author upon reasonable request.

Declaration of generative AI and AI-assisted technologies in the writing process

No generative AI was used in the writing of this manuscript.

Sources of funding

This study was partially funded by the European Union – Next Generation EU, Mission 4 Component 1 (CUP D53D23021100001), under the PRIN PNRR 2022 Call (P2022JBKN2), Italian Ministry of University and Research (MUR).

Declaration of competing interest

The authors declare that they have no known competing financial interests or personal relationships that could have appeared to influence the work reported in this paper.

Appendix A. Supplementary data

Supplementary data to this article can be found online at https://doi.org/10.1016/j.jcct.2026.03.002.

References

1. Faggiano A, Gherbesi E, Carugo S, et al. Prognostic value of myocardial computed tomography–derived extracellular volume in severe aortic stenosis requiring aortic valve replacement: a systematic review and meta-analysis. *Eur Heart J Cardiovasc Imaging*. 2025;26(3):518–531. https://doi.org/10.1093/ehjci/jeae324.
2. Kato S, Misumi Y, Horita N, Yamamoto K, Utsunomiya D. Clinical utility of computed tomography–derived myocardial extracellular volume fraction. *JACC Cardiovasc Imaging*. 2024;17(5):516–528. https://doi.org/10.1016/j.jcmg.2023.10.008.
3. Azevedo CF, Nigri M, Higuchi ML, et al. Prognostic significance of myocardial fibrosis quantification by histopathology and magnetic resonance imaging in patients with severe aortic valve disease. *J Am Coll Cardiol*. 2010;56(4):278–287. https://doi.org/10.1016/j.jacc.2009.12.074.
4. Nacif MS, Kawel N, Lee JJ, et al. Interstitial myocardial fibrosis assessed as extracellular volume fraction with low-radiation-dose cardiac CT. *Radiology*. 2012;264(3):876–883. https://doi.org/10.1148/radiol.12112458.
5. Cundari G, Galea N, Mergen V, Alkadhi H, Eberhard M. Myocardial extracellular volume quantification with computed tomography—current status and future outlook. *Insights Imaging*. 2023;14(1):156. https://doi.org/10.1186/s13244-023-01506-6.
6. Bartoli A, Gnasso C, Palmisano A, Bettinelli A, Vignale D, Esposito A. Myocardial characterization on CT: late iodine enhancement and extracellular volume. *Echocardiography*. 2025;42(2). https://doi.org/10.1111/echo.70108.
7. Vignale D, Palmisano A, Gnasso C, et al. Extracellular volume fraction (ECV) derived from pre-operative computed tomography predicts prognosis in patients undergoing transcatheter aortic valve implantation (TAVI). *Eur Heart J Cardiovasc Imaging*. 2023;24(7):887–896. https://doi.org/10.1093/ehjci/jead040.
8. Tamarappoo B, Han D, Tyler J, et al. Prognostic value of computed tomography–derived extracellular volume in TAVR patients with low-flow low-gradient aortic stenosis. *JACC Cardiovasc Imaging*. 2020;13(12):2591–2601. https://doi.org/10.1016/j.jcmg.2020.07.045.
9. Hammer Y, Talmor-Barkan Y, Abelow A, et al. Myocardial extracellular volume quantification by computed tomography predicts outcomes in patients with severe aortic stenosis. *PLoS One*. 2021;16(3):e0248306. https://doi.org/10.1371/journal.pone.0248306.
10. Liu Y, Liu S, Nacif MS, et al. A framework to measure myocardial extracellular volume fraction using dual-phase low dose CT images. *Med Phys*. 2013;40(10). https://doi.org/10.1118/1.4819936.
11. Koike H, Fukui M, Treibel T, et al. Comprehensive myocardial assessment by computed tomography. *JACC Cardiovasc Imaging*. 2024;17(4):396–407. https://doi.org/10.1016/j.jcmg.2023.08.008.
12. Takahashi M, Takaoka H, Yashima S, et al. Extracellular volume fraction by computed tomography predicts prognosis after transcatheter aortic valve replacement. *Circ J*. 2024;88(4):CJ-23–288. https://doi.org/10.1253/circj.CJ-23-0288.
13. Patel KP, Scully PR, Saberwal B, et al. Regional distribution of extracellular volume quantified by cardiac CT in aortic stenosis: insights into disease mechanisms and impact on outcomes. *Circ Cardiovasc Imaging*. 2024;17(5). https://doi.org/10.1161/CIRCIMAGING.123.015996.
14. Emoto T, Oda S, Kidoh M, et al. Myocardial extracellular volume quantification using cardiac computed tomography: a comparison of the dual-energy iodine method and the standard subtraction method. *Acad Radiol*. 2021;28(5):e119–e126. https://doi.org/10.1016/j.acra.2020.03.019.
15. Kojima T, Yamasaki Y, Nishigake D, et al. Clinical utility of non-gated 4-min delayed dual-energy CT for myocardial extracellular volume quantification. *Br J Radiol*. 2025;98(1168):600–606. https://doi.org/10.1093/bjr/tqaf022.
16. Lorenzatti DA, Filtz A, Piña P, et al. Comparison of dual-energy iodine and standard subtraction methods for myocardial extracellular volume quantification using cardiac computed tomography. *J Cardiovasc Comput Tomogr*. 2025;19(4):483–487. https://doi.org/10.1016/j.jcct.2025.03.009.
17. Wasserthal J, Breit HC, Meyer MT, et al. TotalSegmentator: robust segmentation of 104 anatomic structures in CT images. *Radiol Artif Intell*. 2023;5(5). https://doi.org/10.1148/ryai.230024.
18. Székely GJ, Rizzo ML. The energy of data. *Annu Rev Stat Appl*. 2017;4(1):447–479. https://doi.org/10.1146/annurev-statistics-060116-054026.
19. Gama F, Rosmini S, Bandula S, et al. Extracellular volume fraction by computed tomography predicts long-term prognosis among patients with cardiac amyloidosis. *JACC Cardiovasc Imaging*. 2022;15(12):2082–2094. https://doi.org/10.1016/j.jcmg.2022.08.006.
20. Nitsche C, Scully PR, Patel KP, et al. Prevalence and outcomes of concomitant aortic stenosis and cardiac amyloidosis. *J Am Coll Cardiol*. 2021;77(2):128–139. https://doi.org/10.1016/j.jacc.2020.11.006.
21. Scully PR, Patel KP, Klotz E, et al. Myocardial fibrosis quantified by cardiac CT predicts outcome in severe aortic stenosis after transcatheter intervention. *JACC Cardiovasc Imaging*. 2022;15(3):542–544. https://doi.org/10.1016/j.jcmg.2021.10.016.
22. Bing R, Cavalcante JL, Everett RJ, Clavel MA, Newby DE, Dweck MR. Imaging and impact of myocardial fibrosis in aortic stenosis. *JACC Cardiovasc Imaging*. 2019;12(2):283–296. https://doi.org/10.1016/j.jcmg.2018.11.026.
23. Treibel TA, López B, González A, et al. Reappraising myocardial fibrosis in severe aortic stenosis: an invasive and non-invasive study in 133 patients. *Eur Heart J*. 2018;39(8):699–709. https://doi.org/10.1093/eurheartj/ehx353.
24. Pires LT, Rosa VEE, Morais TC, et al. Postoperative myocardial fibrosis assessment in aortic valvular heart diseases—a cardiovascular magnetic resonance study. *Eur Heart J Cardiovasc Imaging*. 2023;24(7):851–862. https://doi.org/10.1093/ehjci/jead041.
25. Everett RJ, Treibel TA, Fukui M, et al. Extracellular myocardial volume in patients with aortic stenosis. *J Am Coll Cardiol*. 2020;75(3):304–316. https://doi.org/10.1016/j.jacc.2019.11.032.
26. Scully PR, Patel KP, Saberwal B, et al. Identifying cardiac amyloid in aortic stenosis. *JACC Cardiovasc Imaging*. 2020;13(10):2177–2189. https://doi.org/10.1016/j.jcmg.2020.05.029.
27. Palmisano A, Vignale D, Tadic M, et al. Myocardial late contrast enhancement CT in troponin-positive acute chest pain syndrome. *Radiology*. 2022;302(3):545–553. https://doi.org/10.1148/radiol.211288.
28. Esposito A, Palmisano A, Antunes S, et al. Cardiac CT with delayed enhancement in the characterization of ventricular tachycardia structural substrate. *JACC Cardiovasc Imaging*. 2016;9(7):822–832. https://doi.org/10.1016/j.jcmg.2015.10.024.
29. Muthalaly RG, Abrahams T, Lin A, et al. Myocardial extracellular volume measurement using cardiac computed tomography. *Int J Cardiovasc Imaging*. 2024;40(11):2237–2245. https://doi.org/10.1007/s10554-024-03226-4.